ECS Journal of Solid State Science and Technology, **2** (9) R169-R171 (2013)
2162-8769/2013/2(9)/R169/3/$31.00 © The Electrochemical Society

Evolution of Bottom *c*-Plane on Wet-Etched Patterned Sapphire Substrate

Chien-Chih Chen,[a] Feng Ching Hsiao,[a] Bo-Wen Lin,[a,b] Wen-Ching Hsu,[c] and YewChung Sermon Wu[a,*,z]

[a]*Department of Materials Science and Engineering, National Chiao Tung University, Hsinchu, Taiwan*
[b]*Crystalwise Technology Inc., Hsinchu, Taiwan*
[c]*Sino-American Silicon Products Inc., Hsinchu, Taiwan*

Wet-etched pattern sapphire substrate (PSS) has been employed to improve the epitaxy of GaN-based LEDs. It was found that the crystal quality and performance of LEDs improved with decrease in *c*-plane areas of PSS. However, further decrease in bottom *c*-plane areas makes epitaxy of GaN film very difficult. In this research, the evolution of bottom *c*-plane was investigated through a systematic study. It was found that epitaxy difficulty might be due to the appearance of 6C facets $\{4\bar{1}\bar{3}18\}$ and the disappearance of bottom *c*-plane.
© 2013 The Electrochemical Society. [DOI: 10.1149/2.022309jss] All rights reserved.

Manuscript submitted March 28, 2013; revised manuscript received May 30, 2013. Published July 3, 2013.

Light-emitting diodes (LEDs) have been widely used in a variety of applications due to their advantages of high efficiency, long life, small size, environmental protection and various colors. Many techniques have been developed to improve internal quantum efficiency (IQE) and light extraction efficiency (LEE) of GaN-based LEDs. Examples of such techniques include pendeoepitaxy,[1] epitaxial lateral overgrowth (ELOG),[2] surface roughing,[3,4] metal mirror reflect layer[5] and patterned sapphire substrate (PSS).[6–9] In recent years, PSS has attracted much attention because it can improve both IQE and LEE.[10–13]

There are two methods for fabricating PSSs: (1) dry etching and (2) wet etching. In dry etching, ion bombardment damaged PSS surface and increased the threading dislocation density in GaN epitaxial layers.[14] On the other hand, wet etching did not damage PSS surface. Moreover, wet etching is a less expensive method in terms of equipment and process costs.[15]

In wet etching, sapphire substrate covered with SiO_2 hard mask is usually etched with a mixed solution of hot H_2SO_4 and H_3PO_4.[16,17] After etching, PSS has a three-dimensional structure, which is composed of a hexagonal pyramid covered with several etched facets.[18] In our previous two-step etching study, we found that GaN quality improved with decrease in bottom *c*-plane areas from 47.5 to 9.6%.[19] This is because most of the GaN growth was initiated from *c*-plane. As growth time increased, GaN epilayers on the bottom *c*-plane covered these pyramids by lateral growth causing the threading dislocation to bend toward the pyramids.[19–22] As a result, threading dislocation density would decrease with the bottom *c*-plane areas.

However, we also found that further decrease in bottom *c*-plane areas makes epitaxy of GaN film on PSS very difficult. Therefore, the evolution of bottom *c*-plane was investigated in this study.

Experimental

C-plane PSSs with periodic dot array SiO_2 patterns (1-μm width and 2-μm spacing) were prepared by standard photolithography. SiO_2 patterns were 200 nm thick and served as the wet-etching hard mask. Samples were then immersed in a mixed solution of hot H_2SO_4 and H_3PO_4 at 270°C for various durations. It was designated as "tPSS", where t denotes the etching time. The surface morphology was analyzed using scanning electron microscope (SEM), and cross-sectional SEM inspection was achieved after localized etching by focused ion beam (FIB).

Results and Discussion

Figure 1 shows the SEM images of 10PSS with a flat top *c*-plane. The structure of 10PSS comprises a hexagonal pyramid covered with six facets (6B) $\{3\bar{4}17\}$.[18] Among these pyramids, there were some bottom *c*-plane. When etching time was less than 10 min, the PSS morphologies were similar to 10PSS. With increase in etching time, the size/height of pyramids increased while the areas of bottom *c*-plane decreased, as seen in the SEM images of 12PSS (Fig. 2).

When etching time reached 14 min (14PSS), the bottoms of pyramids pinched together. As shown in Fig. 3, beside 6B planes, six new facets were found among bottom *c* and 6B planes for the first time. With increase in etching time, the areas of new facets increased while those of bottom *c*-plane decreased. As the etching time reached around 16 min (16PSS), the bottom *c*-plane disappeared, as shown in Fig. 4. The new six facets were designated as "6-Concavity" (6C) planes. The appearance of 6C planes and the disappearance of bottom *c*-plane might be the reasons why epitaxy of GaN film on PSS turned out to be extremely difficult. The pyramids heights of 10, 12, 14 and 16PSS were 1.34, 1.50, 1.84 and 1.96 μm, respectively. When etching time was greater than 16 min, the pattern morphology (6C facets) changed not much.

A "vacancy" dot array SiO_2 pattern was employed to study these tiny 6C areas. Figure 5 shows the periodic array of vacancy-mask and vacancy-PSS. As can be seen, 6C facets are found among distorted pyramids, and the intersections (edges) of 6C planes and *c*-plane collided with each other, as shown in Fig. 5b and 6b. The high-magnification SEM images of 16PSS and vacancy-PSS are compared in Fig. 6. The corresponding relation of the 6C facets was indicated with numbers from 1 to 6.

The images and related illustration of collided 6C planes are shown in Fig. 7. The top-view (projection) image of 6C planes was a quadrilateral *ABCD*. As shown in Fig. 7a, the projection internal angles of *ABCD* were 60°, 124°, 26° and 150°, respectively. The cross-sectional images of each edge are shown in Figs. 7c - 7f, respectively. Some angles among edges and [001] (normal direction of *c*-plane) were measured and illustrated in Figs. 7d and 7e. According to these

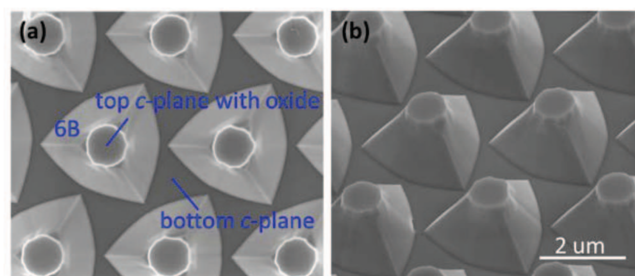

Figure 1. SEM images of 10PSS with SiO_2 layer on top *c*-plane. (a) Top-view image. (b) Side-view image (viewed from 40° to sample normal).

*Electrochemical Society Active Member.
zE-mail: SermonWu@StanfordAlumni.org

Downloaded on 2014-04-27 to IP 140.113.38.11 address. Redistribution subject to ECS terms of use (see ecsdl.org/site/terms_use) unless CC License in place (see abstract).

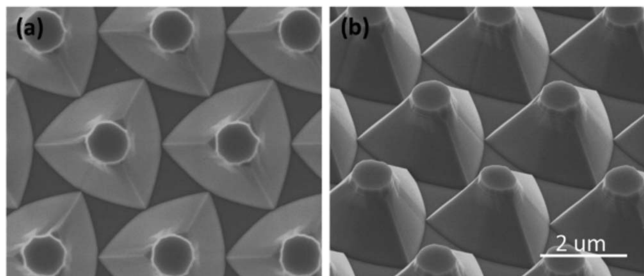

Figure 2. SEM images of 12PSS. (a) Top-view image. (b) Side-view image.

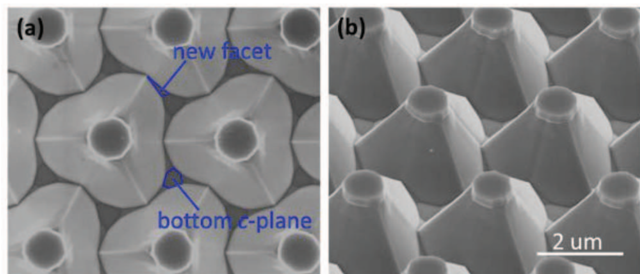

Figure 3. SEM images of 14PSS. (a) Top-view image. (b) Side-view image.

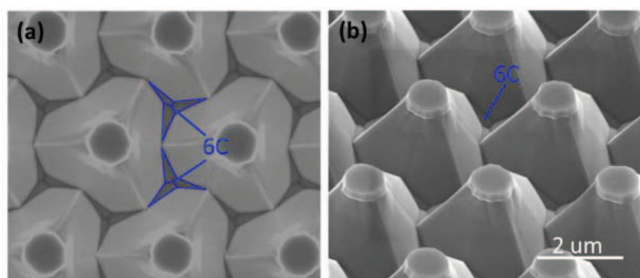

Figure 4. SEM images of 16PSS. (a) Top-view image. (b) Side-view image. The bottom *c*-plane disappeared.

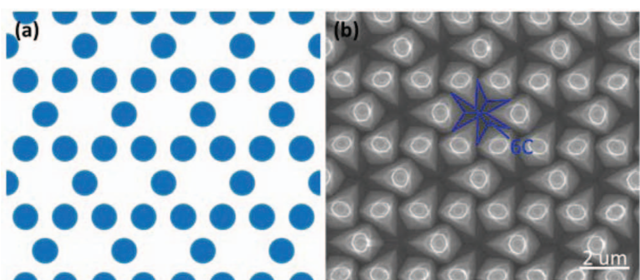

Figure 5. (a) Schematic illustration of vacancy-mask and (b) SEM image of vacancy-PSS.

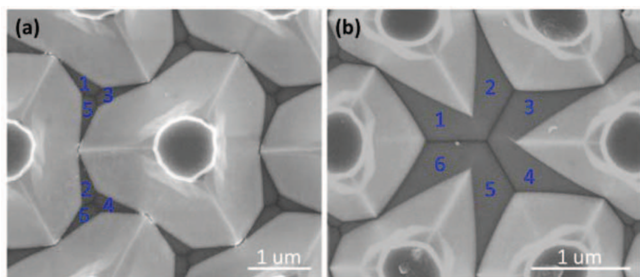

Figure 6. High-magnification SEM images of (a) 16PSS and (b) vacancy-PSS.

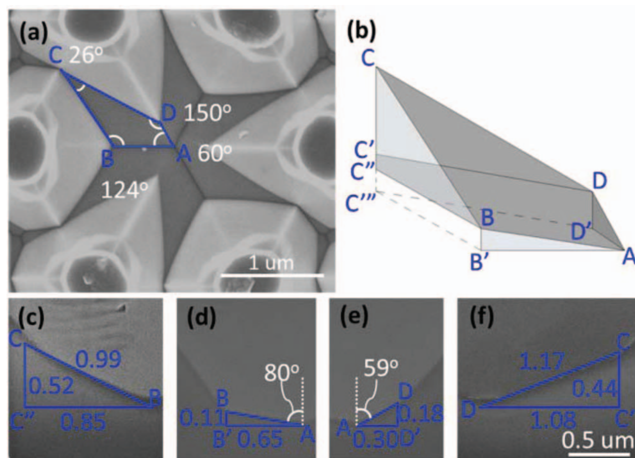

Figure 7. Images and related illustration of collided 6C planes. (a) Top-view (projection) image. (b) 3D schematic illustration of 6C planes. (c), (d), (e) and (f) are side-view images of each edge from (a) (viewed from 52° to sample normal).

observations, a 3D structure of quadrilateral *ABCD* was schematically illustrated in Fig. 7b.

Figure 8 illustrates the crystallographic planes from different view angles and Fig. 8c displays a detailed analysis of a 6C plane. As can be seen, the intercepts of this "extended"6C plane on a_1, a_2 and c axes are about 5.19, −20.76 and 3.15 units, respectively. In hexagonal crystals, the Miller-Bravais indexes of a plane are denoted by *(h k i l)*. These indexes are the reciprocals of intercepts on a_1, a_2, a_3 and c, respectively. The additional condition which their values must satisfy is $h + k = -i$. Take the reciprocals of these numbers, and multiply them with sapphire's unit length (a = 0.4759 nm and c = 1.2991 nm).[18] The calculated Miller-Bravais indexes of 6C planes are $\{4\bar{1}\bar{3}18\}$.

To confirm the indexes of 6C planes, some of these 6C planes [$(\bar{4}3118)$, $(4\bar{1}\bar{3}18)$ and $(31\bar{4}18)$] were illustrated in Fig. 9. The intersection directions of these three planes were calculated by the cross product of normal directions of these planes. As shown in Fig. 9a, they were $\overrightarrow{AD}$ $[\overline{36}\,\overline{18}\,7]$ and $\overrightarrow{AB}$ $[\bar{9}\,\overline{18}\,1]$. The projections of these two

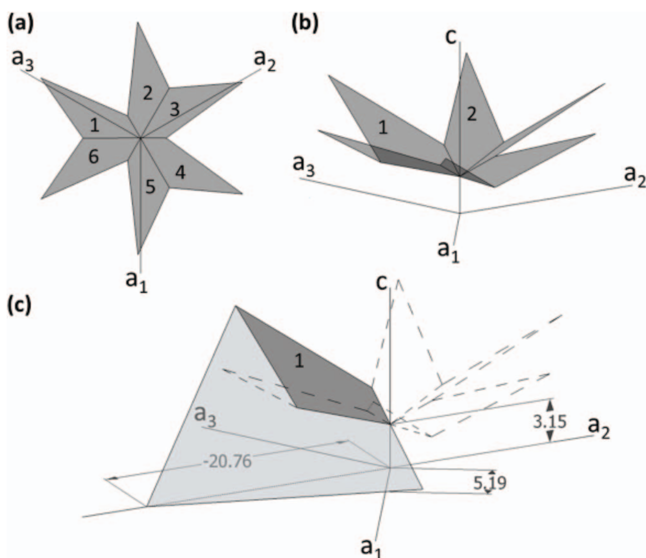

Figure 8. Schematic illustrations of 6C planes. (a) Top-view illustration. (b) Side-view 3D illustration. (c) The intercepts of an "extended" 6C plane on a_1, a_2 and c axes.

Downloaded on 2014-04-27 to IP 140.113.38.11 address. Redistribution subject to ECS terms of use (see ecsdl.org/site/terms_use) unless CC License in place (see abstract).

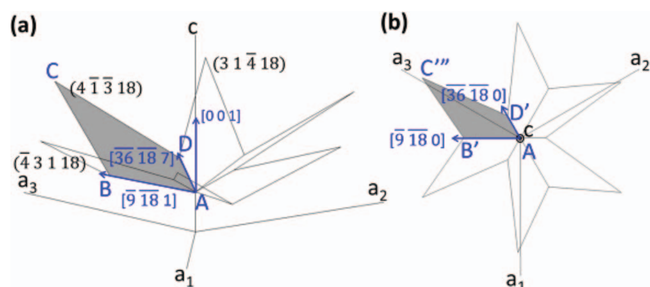

Figure 9. Schematic illustrations of 6C planes with plane indexes and intersection directions. (a) Side-view illustration. (b) Top-view illustration.

directions on (0001) plane were $[\overline{36}\,\overline{18}\,0]$ and $[\bar{9}\,\overline{18}\,0]$ as shown in Fig. 9b.

The angles between two directions in a hexagonal crystal could be calculated by

$$\theta = cos^{-1}\left[\frac{u_1u_2 - \frac{1}{2}(u_1v_2 + u_2v_1) + v_1v_2 + \frac{c^2}{a^2}w_1w_2}{\sqrt{u_1^2 - u_1v_1 + v_1^2 + \frac{c^2}{a^2}w_1^2}\sqrt{u_2^2 - u_2v_2 + v_2^2 + \frac{c^2}{a^2}w_2^2}}\right]$$

where $[u_1\ v_1\ w_1]$ and $[u_2\ v_2\ w_2]$ are the two directions in Miller notation.[18] The calculated angle between these two projection directions was 60°, the same as angle *A* observed in Fig. 7a.

Likewise, the calculated angle between $\overrightarrow{AB}$ $[\bar{9}\,\overline{18}\,1]$ and [0 0 1] is 80.1°, which was almost the same as the angle observed in Fig. 7d. The calculated angle between $\overrightarrow{AD}$ $[\overline{36}\,\overline{18}\,7]$ and [0 0 1] is 58.5°, which was almost the same as the measured angle in Fig. 7e.

Besides the analysis of these collided 6C planes, non-collided 6C planes were also employed to confirm the indexes of 6C planes. As shown in Fig. 10, tiny 6C planes did not collide with each other. The calculated intersection of 6C plane $(4\bar{1}\bar{3}\,18)$ and *c*-plane (0001) was $[\bar{1}\,\bar{4}\,0]$, as illustrated in Fig. 10. The calculated angle between a_1 [001] and $[\bar{1}\,\bar{4}\,0]$ was 73.9°, which was almost the same as the measured angle.

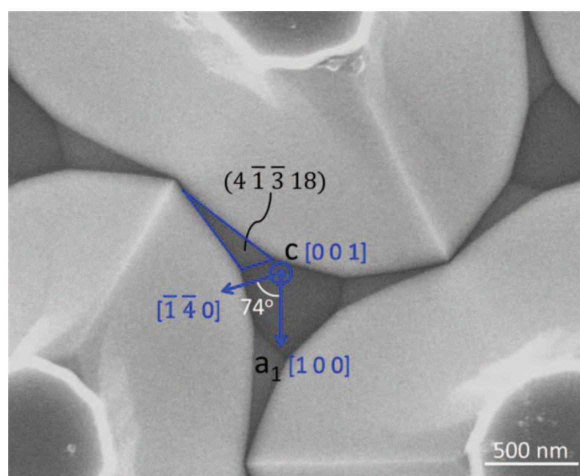

Figure 10. SEM image of intersection of a non-collided 6C plane and *c*-plane. The intersection direction was almost the same as $[\bar{1}\,\bar{4}\,0]$.

Conclusion

Wet-etched PSS has been employed to improve the performance of GaN-based LEDs. Reduction of bottom *c*-plane areas in PSSs can enhance the quality of GaN epitaxial layer.[19] This is because the threading dislocation density decreased with bottom *c*-plane areas. However, further decrease in bottom *c*-plane areas makes epitaxy of GaN film very difficult. In this study, 6C facets were found among bottom *c* and 6B planes for the first time. Their Miller-Bravais indexes were identified as $\{4\bar{1}\bar{3}\,18\}$. With increase in etching time, the areas of 6C facets increased while those of bottom *c*-plane decreased. As the etching time reached around 16 min, the bottom *c*-plane disappeared. The appearance of 6C planes and the disappearance of bottom *c*-plane might be the reasons why the epitaxy of GaN film on PSS turned out to be extremely difficult.

Acknowledgments

This project was funded by Sino American Silicon Products Incorporation and the National Science Council of the Republic of China under grant No. 101-2221-E-009-052-MY3. Technical support from the National Nano Device Laboratory, Center for Nano Science and Technology, Nano Facility Center and Semiconductor Laser Technology Laboratory of the National Chiao Tung University is also gratefully acknowledged.

References

1. K. Linthicum, T. Gehrke, D. Thomson, E. Carlson, P. Rajagopal, T. Smith, D. Batchelor, and R. Davis, *Appl. Phys. Lett.*, **75**, 196 (1999).
2. A. Sakai, H. Sunakawa, and A. Usui, *Appl. Phys. Lett.*, **71**, 2259 (1997).
3. W. C. Peng and Y. S. Wu, *Appl. Phys. Lett.*, **88**, 181117 (2006).
4. C. E. Lee, Y. J. Lee, H. C. Kuo, M. R. Tsai, B. S. Cheng, T. C. Lu, S. C. Wang, and C. T. Kuo, *IEEE Photonics Technol. Lett.*, **19**, 1200 (2007).
5. Y. S. Wu, C. Liao, and W. C. Peng, *Electrochem. Solid-State Lett.*, **10**, J126 (2007).
6. D. S. Wuu, W. K. Wang, K. S. Wen, S. C. Huang, S. H. Lin, R. H. Horng, Y. S. Yu, and M. H. Pan, *J. Electrochem. Soc.*, **153**, G765 (2006).
7. J. H. Lee, J. T. Oh, Y. C. Kim, and J. H. Lee, *IEEE Photonics Technol. Lett.*, **20**, 1563 (2008).
8. C. H. Chiu, H. H. Yen, C. L. Chao, Z. Y. Li, P. Yu, H. C. Kuo, T. C. Lu, S. C. Wang, K. M. Lau, and S. J. Cheng, *Appl. Phys. Lett.*, **93**, 081108 (2008).
9. H. C. Lin, R. S. Lin, J. I. Chyi, and C. M. Lee, *IEEE Photonics Technol. Lett.*, **20**, 1621 (2008).
10. C. Y. Hsieh, B. W. Lin, H. J. Cho, B. M. Wang, and Y. S. Wu, *ECS J. Solid State Sci. Technol.*, **1**, Q35 (2012).
11. Y. J. Lee, T. C. Hsu, H. C. Kuo, S. C. Wang, Y. L. Yang, S. N. Yen, Y. T. Chu, Y. J. Shen, M. H. Hsieh, M. J. Jou, and B. J. Lee, *Mater. Sci. Eng., B*, **122**, 184 (2005).
12. Z. H. Feng and K. M. Lau, *IEEE Photonics Technol. Lett.*, **17**, 1812 (2005).
13. Y. J. Lee, J. M. Hwang, T. C. Hsu, M. H. Hsieh, M. J. Jou, B. J. Lee, T. C. Lu, H. C. Kuo, and S. C. Wang, *IEEE Photonics Technol. Lett.*, **18**, 1152 (2006).
14. M. Kappelt and D. Bimberg, *J. Electrochem. Soc.*, **143**, 3271 (1996).
15. Y. J. Lee, H. C. Kuo, T. C. Lu, B. J. Su, and S. C. Wang, *J. Electrochem. Soc.*, **153**, G1106 (2006).
16. F. Dwikusuma, D. Saulys, and T. F. Kuech, *J. Electrochem. Soc.*, **149**, G603 (2002).
17. H. Gao, F. Yan, Y. Zhang, J. Li, Y. Zeng, and G. Wang, *J. Appl. Phys.*, **103**, 014314 (2008).
18. Y. C. Chen, F. C. Hsiao, B. W. Lin, B. M. Wang, Y. S. Wu, and W. C. Hsu, *J. Electrochem. Soc.*, **159**, D362 (2012).
19. J. H. Cheng, Y. S. Wu, W. C. Liao, and B. W. Lin, *Appl. Phys. Lett.*, **96**, 051109 (2010).
20. Q. Dai, M. F. Schubert, M. H. Kim, J. K. Kim, E. F. Schubert, D. D. Koleske, M. H. Crawford, S. R. Lee, A. J. Fischer, G. Thaler, and M. A. Banas, *Appl. Phys. Lett.*, **94**, 111109 (2009).
21. J. H. Lee, J. T. Oh, J. S. Park, J. W. Kim, Y. C. Kim, J. W. Lee, and H. K. Cho, *Phys. Status Solidi C*, **3**, 2169 (2006).
22. C. C. Pan, C. H. Hsieh, C. W. Lin, and J. I. Chyi, *J. Appl. Phys.*, **102**, 084503 (2007).

Downloaded on 2014-04-27 to IP 140.113.38.11 address. Redistribution subject to ECS terms of use (see ecsdl.org/site/terms_use) unless CC License in place (see abstract).